

Supplemental Material to: Spin- and momentum-correlated atom pairs mediated by photon exchange and seeded by vacuum fluctuations

Fabian Finger,^{1,*} Rodrigo Rosa-Medina,^{1,*} Nicola Reiter,¹
Panagiotis Christodoulou,¹ Tobias Donner,^{1,†} and Tilman Esslinger¹

¹*Institute for Quantum Electronics, ETH Zürich, 8093 Zürich, Switzerland*

EXPERIMENTAL DETAILS

We operate the drive laser at 790.019 nm, i.e., the ^{87}Rb D-line tune-out wavelength [1], where the scalar ac-Stark shift vanishes for $F = 1$. This suppresses dipole potentials and minimizes spontaneous emission, otherwise relevant for the operating powers ~ 100 mW. We experimentally verify that the drive does not induce significant losses by monitoring the atom-number evolution while illuminating with the maximum experimentally used laser power. The measured $1/e$ lifetime of 47(7) ms is orders of magnitude larger than our relevant experimental timescales of ~ 100 μs . Note that during this measurement we keep the cavity unlocked to avoid cavity-induced interactions. The drive polarization is chosen along y to inhibit atomic self-organization in the $m = \pm 1$ sublevels mediated by the vectorial polarizability [2].

Our optical cavity is a quasi-planar symmetric Fabry-Perot resonator with a length of 176 μm and finesse $\mathcal{F} = 3.5 \cdot 10^5$; the TEM_{00} mode has a waist of $w_c = 25$ μm . The cavity is actively stabilized by locking the resonance to the frequency of a reference laser with wavelength of 830 nm using a Pound-Drever-Hall technique; the 830 nm laser is referenced to the laser generating the transverse pump beams via locking on a transfer cavity.

In Table S1, we list all relevant experimental parameters for the measurements shown in this work. For the measurements of Fig. 4(b-c) in the main text, we adjust the drive power P and thus $\eta \propto \sqrt{P}$ to keep $\chi_{+, \text{fix}} = -2\pi \times 0.50(2)$ Hz constant. We calibrate P using Kapitza-Dirac diffraction [3]. Following Refs. [4, 5], we tune the drive away from the tune-out wavelength and illuminate the atoms in a standing-wave configuration.

Fig.	$N (\times 10^4)$	$t (\mu\text{s})$	$\omega_z/2\pi$ (MHz)	$\delta_+/2\pi$ (MHz)	$\chi_+/2\pi$ (Hz)
1(c)		65	7.09(1)	-20.7(3)	-0.50(1)
2(a,c)	4.0(3)	60	7.09(1)	-18.7(3)	-0.43(2)
2(b,d)	5.3(4)	62	1.01(1)	-18.7(3)	-0.43(2)
3(a)	7.2(6)	62	7.09(1)	-25.7(3)	-0.33(1)
3(b)	7.0(6)	62	0.90(1)	-25.7(1)	-0.33(1)
4(a)	8.1(3)		7.09(1)	-22.7(1)	-0.21(1)
4(b,c)	7.9(3)	80	7.09(1)		-0.50(2)

TABLE S1. List of experimental parameters.

DETECTION AND CALIBRATION OF ATOM POPULATIONS

We measure the momentum distribution by shining a high-intensity imaging beam along y on the atoms after 5.5–6.2 ms of time-of-flight (TOF) expansion. To spatially resolve atoms in the different m sublevels, we apply a magnetic field gradient along z during TOF (Stern-Gerlach separation). We extract the atom populations in the different spin and momentum states from circular-shaped crops in the absorption images. For that, we correct for short-scale intensity variations in the imaging-beam profile [6]. Such variations mainly originate from diffraction effects on the cavity which acts as a thick slit for the light. Our detection is finally calibrated with a systematic uncertainty of $\sim 15\%$ using the dispersive shift of the cavity resonance in the presence of a $m = 0$ BEC [7]. We additionally verify the absence of significant m -dependent effects on atom counting. To do so, we drive an initially polarized BEC in $m = -1$ in a three-level Rabi oscillation and observe a constant total atom number while the populations of the three m states change.

The technical detection noise in our system is well captured by a Gaussian distribution [8] as shown by the fit in the right panel of Fig. 2(c) in the main text, yielding a standard deviation of $\sigma_{\text{det}} \approx 200$. The distributions are then fit by a convolution of a Bose-Einstein distribution $p_{\text{BE}}(N_p, \langle N_p \rangle)$ and a normalized Gaussian $G(N_p, \sigma_G, \mu)$

$$p(N_p, \langle N_p \rangle, \sigma_G, \mu) = p_{\text{BE}}(N_p, \langle N_p \rangle) * G(N_p, \sigma_G, \mu), \quad (\text{S1})$$

where $\langle N_p \rangle$ is the mean pair number extracted from the raw distribution and σ_G and μ remain fit parameters to capture position-dependent noise effects; we find $\sigma_G \approx \sigma_{\text{det}}$. Assuming uncorrelated physical and technical fluctuations, we estimate the standard deviation of the pair histograms as $\sigma(N_p) = \sqrt{\sigma_{\text{exp}}^2(N_p) - \sigma_G^2}$, where $\sigma_{\text{exp}}(N_p)$ is the experimentally measured standard deviation.

HETERODYNE DETECTION

We monitor the photon field leaking out of the cavity by separating the y - and z -polarizations on a polarizing

beamsplitter, and detecting each of them with independent heterodyne setups. The latter is used to produce the data discussed in this work: the cavity light field originating from superradiant Raman scattering (at frequency ω_{SR}) is fiber coupled and interfered with a local oscillator laser (ω_{LO}). The high detection bandwidth of 250 MS/s allows for an all-digital demodulation of the beat notes over a broad frequency range of $2\pi \times [0, 125]$ MHz, facilitating frequency-resolved detection of superradiant photon pulses associated with both scattering channels.

The complex intra-cavity field $\alpha(t) = X(t) + iY(t)$ is obtained from the quadratures $X(t)$ and $Y(t)$ after digital demodulation at a desired target frequency $\omega_T = \omega_{\text{SR}} - \omega_{\text{LO}}$. Then, the corresponding power spectral density, $\text{PSD}(\omega) = |\text{FFT}(\alpha)|^2(\omega)$, is calculated using a fast Fourier-transform of the form $\text{FFT}(\alpha)(\omega) = dt/\sqrt{\tilde{N}} \sum_j \alpha^*(t_j) e^{-i\omega t_j}$, where t_j is the time of the j^{th} step and \tilde{N} is the total number of steps in the integration window. The traces are divided in time intervals of $T = 150 \mu\text{s}$ with an overlap of 50% between subsequent intervals, with the photon number spectrogram being calculated as $\tilde{n}_{\text{ph}}(t, \omega) = \text{PSD}(\omega)/T$.

To compute the average photon number traces $n_{\text{ph}}(t)$ around the target frequency ω_T , we integrate the photon number spectrogram over a small frequency region of $\Omega = 2\pi \times [-200, +200]$ kHz, and obtain

$$n_{\text{ph}}(t) = \sum_{\Omega} \tilde{n}_{\text{ph}}(t, \omega). \quad (\text{S2})$$

Finally, the total number of photons associated with superradiant scattering presented in Fig. 4(b) is obtained by numerically integrating the photon traces in time

$$\langle N_{\text{ph}} \rangle = 2\kappa \int_0^\infty n_{\text{ph}}(t) dt, \quad (\text{S3})$$

with $\kappa = 2\pi \times 1.25$ MHz being the cavity field losses.

EXPERIMENTAL TIMESCALES

The characteristic timescale to produce pairs, $T_{\text{int}} = 2\pi/(N\max|\chi_{\pm}|)$, is determined by the collective couplings $N\chi_{\pm}$. For typical values of $N \approx 6 \times 10^4$ and $\chi_+ \approx -2\pi \times 0.4$ Hz, we obtain $T_{\text{int}} \approx 40 \mu\text{s}$. On the other hand, the lifetime of the pairs is limited by the harmonic trapping potential since the paired states with $\pm\hbar k$ are not trap eigenstates. We estimate the lifetime as $T_{\text{LT}} = \min(T_{\text{exp}}, T_{\text{sep}})$ [9], with $T_{\text{exp}} = 2\pi/\max(\omega_{hx}, \omega_{hz})$ and $T_{\text{sep}} = R_{\text{TF}}/v_{\text{rec}}$ being the characteristic timescales for the expansion in the harmonic trap and for the separation between the pairs and the zero-momentum BEC, respectively. Using the trap frequencies $[\omega_{hx}, \omega_{hy}, \omega_{hz}] = 2\pi \times [204(3), 34(2), 185(1)]$ Hz, the recoil velocity $v_{\text{rec}} = 0.0058$ m/s and a Thomas-Fermi radius of $R_{\text{TF}} \approx 5.8 \mu\text{m}$, we obtain $T_{\text{exp}} \approx 5$ ms

and $T_{\text{LT}} = T_{\text{sep}} \approx 1$ ms. The separation of timescales, quantified as $T_{\text{LT}}/T_{\text{int}} \approx 25$ and $T_{\text{LT}}/T_{\text{coh}} \approx 6.7$, ensures that pairs are produced in well-defined individual momentum modes and remain in such throughout the entire dynamics. For comparison, collisionally induced pairs in metastable Helium BECs exhibit a ratio of $T_{\text{LT}}/T_{\text{int}} = 0.7$ [9], while for Floquet-engineered systems $T_{\text{LT}}/T_{\text{int}} \lesssim 3$ [10]. Notably, these experiments operate in the spontaneous and weak collective regimes for pair production, respectively.

THERMAL OCCUPATION OF THE PAIRED MODES

We estimate an upper bound for the thermal occupation of the momentum modes forming pairs and conclude that it is negligible compared to quantum fluctuations ($\mathcal{O}(1)$). In our system, with $N \approx 8 \times 10^4$ and a mean trap frequency $\bar{\omega} = (\omega_{hx}\omega_{hy}\omega_{hz})^{1/3} = 2\pi \times 109$ Hz, we get a critical temperature $T_c \approx 210$ nK, and thus a realistic estimation for the cloud's temperature $T \lesssim 100$ nK for a condensate fraction of $N_c/N \gtrsim 0.9$ [7]. Due to a Thomas-Fermi density profile, the momentum-space spread of the initial BEC and the produced modes is $\delta k = 2\pi/R_{\text{TF}} \approx 0.12k$, in agreement with our absorption images. Taking into account the width δk of the paired modes, the probability to thermally occupy each of them is

$$P = 2 \int_{k-\delta k}^{k+\delta k} \int_{-\delta k}^{\delta k} \int_{k-\delta k}^{k+\delta k} p(\mathbf{k}, T) dk_x dk_y dk_z \approx 2.8 \times 10^{-4} \quad (\text{S4})$$

for $T = 100$ nK, where $p(\mathbf{k}, T) = \mathcal{N} \left[\exp\left(\frac{E(\mathbf{k})}{k_B T}\right) + 1 \right]^{-1}$ is the momentum-space probability distribution for the thermal ^{87}Rb atoms of mass M . Here $E(\mathbf{k}) = \hbar^2 \mathbf{k}^2/(2M)$ is the kinetic energy associated with the momenta $\hbar \mathbf{k} = \hbar(k_x, k_y, k_z)$, k_B the Boltzmann constant and \mathcal{N} a suitable normalization factor.

In our experiment, we prepare a BEC solely in $m = 0$ as the initial step for the generation of pairs by applying a strong magnetic-field gradient to clean spurious atoms in $m = \pm 1$ [2]. From our detection, we can safely assume that the population $N_{\pm 1}$ of these sublevels is $< 3\sigma_{\text{det}}$, which lies within the 99.7% confidence interval of our detection, and thus a total number of thermal atoms in $m = \pm 1$ of $N_{\pm 1}^T < (N - N_c)/N \times 3\sigma_{\text{det}} = 60$. The average number of thermal atoms occupying the modes $|\pm k\rangle_{\pm 1}$ is then $\langle N_T \rangle = P N_{\pm 1}^T < 0.016 \ll \mathcal{O}(1)$.

DERIVATION OF THE MANY-BODY HAMILTONIAN

The Hamiltonian of a single atom dispersively coupled to a single cavity mode by a running-wave laser drive is

$$\hat{H}_{\text{SP}} = \frac{\hat{p}^2}{2M} - \hbar\omega_z \hat{F}_z + \hbar q \hat{F}_z^2 + \hbar\omega_c \hat{a}^\dagger \hat{a} - i \frac{\alpha_v}{2F} \left[\hat{\mathbf{E}}^{(+)} \times \hat{\mathbf{E}}^{(-)} \right] \cdot \hat{\mathbf{F}}. \quad (\text{S5})$$

Here, the first term denotes the kinetic energy of the atom, $\omega_z/B = 2\pi \times 700$ kHz/G and $q/B^2 = 2\pi \times 72$ Hz/G² are the linear and quadratic Zeeman splittings, and $\hat{\mathbf{F}} = (\hat{F}_x, \hat{F}_y, \hat{F}_z)^T$ is the spin operator for the $F = 1$ manifold. The operator \hat{a}^\dagger creates a photon in the z -polarized cavity mode of frequency ω_c . Because of our choice of drive wavelength, we consider atom-light interactions mediated only by the vectorial polarizability α_v . The cavity mode extends along x and has a field amplitude $E_0 = 403$ V/m per photon [4]. With E_d indicating the amplitude of the drive with frequency ω_d propagating along $+z$, the negative part of the total electric field is represented by

$$\hat{\mathbf{E}}^{(-)} = \frac{E_d}{2} e^{ikz} e^{-i\omega_d t} \mathbf{e}_y + E_0 \cos(kx) \hat{\mathbf{a}} \mathbf{e}_z, \quad (\text{S6})$$

with unit vectors \mathbf{e}_j , $j \in \{x, y, z\}$. A unitary transformation $\hat{U} = e^{i\hat{H}_{\text{rot}}t/\hbar}$ with $\hat{H}_{\text{rot}} = \hbar\omega_d \hat{a}^\dagger \hat{a} - \hbar\omega_z \hat{F}_z$, and a global phase rotation $\hat{a} \rightarrow \hat{a} e^{i\pi/2}$ gives

$$\hat{H}_{\text{SP}} = \frac{\hat{p}^2}{2M} - \hbar\delta_c \hat{a}^\dagger \hat{a} + \hbar q \hat{F}_z^2 + \frac{\alpha_v E_0 E_d \cos(kx)}{8} \left[(\hat{a}^\dagger e^{ikz} - \hat{a} e^{-ikz}) (\hat{F}_+ e^{-i\omega_z t} + \hat{F}_- e^{i\omega_z t}) \right], \quad (\text{S7})$$

with a drive-cavity detuning $\delta_c = \omega_d - \omega_c$. Note that $|\delta_c| < 2\pi \times 10$ MHz is small compared to the frequency of the drive, and thus we assume a common wavenumber k for the drive and the cavity. We derive the many-body Hamiltonian using a six-mode expansion in momentum and spin space. The selected modes comprise $|0\rangle_0$, with a single-particle wavefunction $\psi \propto 1$, the four modes $|(\pm)k\rangle_{\pm 1}$ occupied by pairs, with $\psi \propto \cos(kx) e^{(\pm)ikz}$, and the next-order mode $\{k_x, k_z, m\} = \{\pm 2k, 0, 0\} \equiv |\pm 2k\rangle_0$, with $\psi \propto \cos^2(kx)$. The latter participates due to the interaction between pairs in $m = \pm 1$. The corresponding spinor field operator is

$$\hat{\Psi}(\mathbf{x}) = \left(\hat{\Psi}_{+1}(\mathbf{x}), \hat{\Psi}_0(\mathbf{x}), \hat{\Psi}_{-1}(\mathbf{x}) \right)^T = \begin{pmatrix} \frac{k}{\sqrt{2\pi}} \cos(kx) (e^{ikz} \hat{c}_{+k,+1} + e^{-ikz} \hat{c}_{-k,+1}) \\ \frac{k}{2\pi} \hat{c}_{0,0} + \frac{\sqrt{2k}}{\sqrt{3\pi}} \cos^2(kx) \hat{c}_{\pm 2k,0} \\ \frac{k}{\sqrt{2\pi}} \cos(kx) (e^{-ikz} \hat{c}_{-k,-1} + e^{ikz} \hat{c}_{+k,-1}) \end{pmatrix}, \quad (\text{S8})$$

where the operators $\hat{c}_{\tilde{k},m}$ follow the main-text definitions.

If the two-photon detunings $\delta_{\pm} = \delta_c \pm \omega_z = (\omega_d \pm \omega_z) - \omega_c = \omega_{\pm} - \omega_c$ significantly exceed the decay rate κ , superradiant Raman scattering from $m = 0$ to $m = \pm 1$ is suppressed. We adiabatically eliminate the cavity field following the formalism of Ref. [11] and obtain the effective many-body Hamiltonian

$$\begin{aligned} \hat{H} &= \hat{H}_0 + \hat{H}_+ + \hat{H}_-, \quad \text{with} \\ \hat{H}_0 &= \hbar \frac{\omega_0}{2} (\hat{c}_{+k,+1}^\dagger \hat{c}_{+k,+1} + \hat{c}_{-k,+1}^\dagger \hat{c}_{-k,+1} \\ &\quad + \hat{c}_{-k,-1}^\dagger \hat{c}_{-k,-1} + \hat{c}_{+k,-1}^\dagger \hat{c}_{+k,-1}) \\ &\quad + 4\hbar\omega_{\text{rec}} \hat{c}_{\pm 2k,0}^\dagger \hat{c}_{\pm 2k,0}, \\ \hat{H}_+ &= \hbar\chi_+ (2\hat{c}_{-k,-1}^\dagger \hat{c}_{+k,+1}^\dagger \hat{c}_0 \hat{c}_0 + \hat{c}_0^\dagger \hat{c}_{+k,+1} \hat{c}_{+k,+1}^\dagger \hat{c}_0 \\ &\quad + \hat{c}_{-k,-1}^\dagger \hat{c}_0 \hat{c}_0^\dagger \hat{c}_{-k,-1} + \text{h.c.}), \\ \hat{H}_- &= \hbar\chi_- (2\hat{c}_{-k,+1}^\dagger \hat{c}_{+k,-1}^\dagger \hat{c}_0 \hat{c}_0 + \hat{c}_0^\dagger \hat{c}_{+k,-1} \hat{c}_{+k,-1}^\dagger \hat{c}_0 \\ &\quad + \hat{c}_0^\dagger \hat{c}_{+k,-1} \hat{c}_{+k,-1}^\dagger \hat{c}_0 + \text{h.c.}), \end{aligned} \quad (\text{S9})$$

where we additionally use the notation $\hat{c}_0 = (\hat{c}_{0,0} + \sqrt{\frac{2}{3}} \hat{c}_{\pm 2k,0})$. The four-photon coupling rates, given in the main text, depend on the two-photon Raman couplings $\eta = \beta \alpha_v E_0 E_d / 8\hbar$. The factor $\beta \approx 0.89$ arises from the overlap integrals between the harmonically confined atomic cloud, the cavity mode and the drive [4]. In the \hat{H}_{\pm} terms, the first part describes the production of pairs in $m = \pm 1$ starting from $m = 0$, while the second (third) describes spin-exchange interactions between $m = 0 \leftrightarrow m = 1$ ($m = 0 \leftrightarrow m = -1$). In presenting the Hamiltonian in Eq. (2) of the main text we omit the latter parts, as spin-exchange dynamics is suppressed when the majority of the atoms populate the pump mode. In the simulations, however, we take into account the full Hamiltonian.

CAVITY DISSIPATION AND EQUATIONS OF MOTION

The leakage of the cavity field makes our experiment intrinsically an open quantum system. We identify effective Lindblad terms

$$\hat{L}_{\pm} = \sqrt{\gamma_{\pm}} \left(\hat{c}_{+k,\pm 1}^\dagger \hat{c}_0 + \hat{c}_0^\dagger \hat{c}_{-k,\mp 1} \right), \quad (\text{S10})$$

which we derive within the framework of the effective operator formalism [11]. The term \hat{L}_{\pm} describes a superradiant Raman decay process, where atoms scatter photons into the cavity while changing their spin state $m \rightarrow m \pm 1$ and obtaining net recoil momentum $+\hbar k$ along z . These cavity photons get lost before they can be further rescattered. The dynamics of the open quan-

tum system is determined by the master equation

$$\frac{d\hat{\rho}}{dt} = -\frac{i}{\hbar} [\hat{H}, \hat{\rho}] + \sum_{j \in \{+, -\}} \hat{L}_j \hat{\rho} \hat{L}_j^\dagger - \frac{1}{2} \left(\hat{L}_j^\dagger \hat{L}_j \hat{\rho} + \hat{\rho} \hat{L}_j^\dagger \hat{L}_j \right). \quad (\text{S11})$$

We define complex-valued expectation values $\psi_{\vec{k}, m} = \langle \hat{c}_{\vec{k}, m} \rangle$ for the different modes and derive mean-field equations of motion (EOM)

$$\begin{aligned} \frac{d}{dt} \psi_{0,0} &= -i\chi_+ (2\psi_0^* \psi_{-k,-1} \psi_{+k,+1} + \psi_{+k,+1}^* \psi_0 \psi_{+k,+1} + \psi_{-k,-1}^* \psi_0 \psi_{-k,-1}) \\ &\quad -i\chi_- (2\psi_0^* \psi_{+k,-1} \psi_{-k,+1} + \psi_{-k,+1}^* \psi_0 \psi_{-k,+1} + \psi_{+k,-1}^* \psi_0 \psi_{+k,-1}) \\ &\quad +\gamma_+ (\psi_{+k,+1}^* \psi_{+k,+1} \psi_0 - \psi_{-k,-1}^* \psi_{-k,-1} \psi_0) \\ &\quad +\gamma_- (\psi_{+k,-1}^* \psi_{+k,-1} \psi_0 - \psi_{-k,+1}^* \psi_{-k,+1} \psi_0) \\ \frac{d}{dt} \psi_{\pm k, \pm 1} &= -i\frac{\omega_0}{2} \psi_{\pm k, \pm 1} \\ &\quad \pm (\gamma_+ \mp i\chi_+) (\psi_0^* \psi_0 \psi_{\pm k, \pm 1} + \psi_{\mp k, \mp 1}^* \psi_0 \psi_0) \\ \frac{d}{dt} \psi_{\mp k, \pm 1} &= -i\frac{\omega_0}{2} \psi_{\mp k, \pm 1} \\ &\quad \pm (\gamma_- \mp i\chi_-) (\psi_0^* \psi_0 \psi_{\mp k, \pm 1} + \psi_{\pm k, \mp 1}^* \psi_0 \psi_0) \\ \frac{d}{dt} \psi_{\pm 2k_x, 0} &= -4i\omega_{\text{rec}} \psi_{\pm 2k_x, 0} \\ &\quad + \sqrt{\frac{2}{3}} [-i\chi_+ (2\psi_0^* \psi_{-k,-1} \psi_{+k,+1} + \psi_{+k,+1}^* \psi_0 \psi_{+k,+1} + \psi_{-k,-1}^* \psi_0 \psi_{-k,-1}) \\ &\quad -i\chi_- (2\psi_0^* \psi_{+k,-1} \psi_{-k,+1} + \psi_{-k,+1}^* \psi_0 \psi_{-k,+1} + \psi_{+k,-1}^* \psi_0 \psi_{+k,-1}) \\ &\quad +\gamma_+ (\psi_{-k,-1}^* \psi_0 \psi_{-k,-1} - \psi_{+k,+1} \psi_0 \psi_{+k,+1}^*) \\ &\quad +\gamma_- (\psi_{+k,-1}^* \psi_0 \psi_{+k,-1} - \psi_{-k,+1} \psi_0 \psi_{-k,+1}^*)]. \end{aligned} \quad (\text{S12})$$

TRUNCATED WIGNER SIMULATIONS

We employ truncated Wigner simulations to model the dynamics of our system in the presence of technical and quantum fluctuations, closely following the methodology proposed for interacting Bose gases in Ref. [12]. Within this approximation, the system is truncated to relevant empty excitation modes \hat{c}_q that are represented by stochastic complex variables ψ_q , with $\hat{c}_q \in \{\hat{c}_{+k,+1}, \hat{c}_{-k,-1}, \hat{c}_{-k,+1}, \hat{c}_{+k,-1}, \hat{c}_{\pm 2k_x, 0}\}$. If the occupation of the different modes is initially uncorrelated, they can be sampled from suitable Gaussian-shaped Wigner distributions with mean $\langle \psi_q \rangle = 0$, and standard deviations $\sigma[\text{Re}(\psi_q)] = 1/2$ and $\sigma[\text{Im}(\psi_q)] = 1/2$. This yields effective initial occupations of

$$\langle N_{\text{QF}} \rangle = \langle \hat{c}_q^\dagger \hat{c}_q \rangle = \langle \psi_q^* \psi_q \rangle = 1/2 \quad (\text{S13})$$

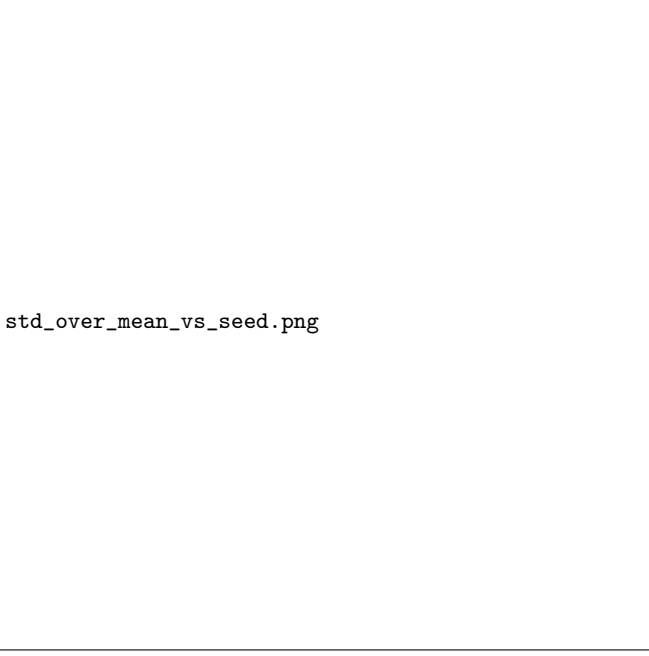
for the empty excitation modes, typically referred to as *quantum one-half fluctuations* and interpreted as the degree of vacuum noise relevant for the dynamics of the system [13].

We initialize all the atoms in the mode $\hat{c}_{0,0}$ by setting $\psi_{0,0}(t=0) = \sqrt{N}$, and sample all the other modes from complex-valued normal distributions with $\mu = 0$ and $\sigma[\text{Re}(\psi_q)] = \sigma[\text{Im}(\psi_q)] = 1/2$. Practically, we sample > 500 different initial conditions for the mean-field EOM in Eq. (S12), which we then numerically evolve using built-in MATLAB methods. We also incorporate shot-to-shot fluctuations of the initial atom number, on the order of $\Delta N/N = 0.05$. We sample the atom number for each simulation from a Gaussian distribution with mean N and standard deviation $\sigma(N) = 0.05N$. Finally, we estimate the expectation value $\langle \hat{O}(t) \rangle$ and the variance $\sigma^2[\hat{O}(t)]$ of the observable $\hat{O}(t)$ at any given time t by averaging over the different samples.

SIMULATED STATISTICS FOR VACUUM-STIMULATED PAIR PRODUCTION AND CLASSICAL SEEDS

The highly nonlinear amplification of pair production allows to characterize the nature of the initial quantum state by measuring the resulting pair statistics after a quench. For this purpose, we perform truncated Wigner simulations with a variable number of classical pairs N_p^s seeding the dynamics. Practically, we sample the individual simulations from Gaussian distribution with $\mu[\text{Re}(\psi_q)] = \sqrt{N_p^s}$. In Fig. S1, we plot the ratio of the standard deviation $\sigma(N_p)$ and the mean pair number $\langle N_p \rangle$ for an initial vacuum state ($N_p^s = 0$) and different classical coherent states ($N_p^s > 0$) as a function of quench time t from 500 simulations. We observe that for an initial vacuum state ($N_p^s = 0$), this ratio is close to unity as expected for a Bose-Einstein distribution. Already a small classical seed comprising a single pair ($N_p^s = 1$) results in a significant reduction of $\sigma(N_p)/\langle N_p \rangle$, as the mean pair number is over-proportionally amplified compared to the quantum fluctuations of the corresponding coherent state; larger seeds further enhance this effect. For quench times up to $t \lesssim 40 \mu\text{s}$, the undepleted pump approximation is well-justified and the ratio stays approximately flat. At the experimental quench time $t = 60 \mu\text{s}$ employed for our measurements in Fig. 2 of the main text, pump depletion becomes non-negligible and results in a reduction of the mean-to-standard deviation ratio, especially for the classically seeded dynamics. This regime is particularly sensitive to small classical seeds, since the resulting pair number distributions are strongly altered.

In Fig. S2, we present simulated histograms obtained from vacuum fluctuations and different classical seeds for early and experimentally relevant quench times. For the short quench time $t = 30 \mu\text{s}$, we observe the expected Bose-Einstein distribution for vacuum-seeded dynamics with $\langle N_p \rangle \approx \sigma(N_p)$, see Fig. S2(a1). Even a classical seed



std_over_mean_vs_seed.png

FIG. S1. Simulated ratio of standard deviation to mean number of pairs $\sigma(N_p)/\langle N_p \rangle$ for an initial vacuum state and different classical seeds N_p^s as a function of quench time t . The vertical gray lines mark the times of the histograms shown in Fig. S1. For the parameters of the truncated Wigner simulations, see Tab. S1 and Fig. 2(c) in the main text.

of one pair $N_p^s = 1$ is sufficient to significantly alter the histogram's shape, whereas a seed of $N_p^s = 5$ additionally shifts the mean significantly, see Figs. S2(a2-a3). For the experimentally relevant quench time $t = 60 \mu\text{s}$, these effects become more pronounced, as also the skewness of the distributions progressively changes from positive to negative with increasing seeds, see Fig. S2(b1-b3). To directly compare these simulations with our experimental results, we convolve the simulated histograms with our Gaussian detection noise $G(N_p, \sigma_G, \mu)$, see Fig. S2(c1-c3) and Fig. 2(e) of the main text. Effectively, the convolution (see also Eq. (S1)) smooths and slightly shifts the distributions while preserving their characteristic shape important for revealing vacuum-seeded dynamics.

ANALOGY TO SPONTANEOUS PARAMETRIC DOWN-CONVERSION

In the following, we elaborate on the analogy between our two-channel configuration, spontaneous parametric down-conversion (SPDC) and Bell states, closely following the approach outlined in Refs. [14, 15]. The interaction Hamiltonian for the two-channel configuration using

the undepleted pump approximation $\hat{c}_{0,0} \approx \sqrt{N}$ reads:

$$\begin{aligned} \hat{H}_{\text{int}} &= \hat{H}_+ + \hat{H}_- \\ &\approx 2\hbar N \chi_+ (\hat{c}_{-k,-1}^\dagger \hat{c}_{+k,+1}^\dagger + \text{h.c.}) \\ &\quad + 2\hbar N \chi_- (\hat{c}_{-k,+1}^\dagger \hat{c}_{+k,-1}^\dagger + \text{h.c.}), \end{aligned} \quad (\text{S14})$$

where we neglect the spin exchange terms. With the definitions $g_\pm = 2N\chi_\pm$, we can rewrite Eq. (S14) in the well-known form of non-collinear, type-II SPDC [16]

$$H_{\text{SPDC}} = \hbar \left(g_+ \hat{c}_{-k,-1}^\dagger \hat{c}_{+k,+1}^\dagger + g_- \hat{c}_{-k,+1}^\dagger \hat{c}_{+k,-1}^\dagger \right) + \text{h.c.}, \quad (\text{S15})$$

where the spin states $m = \pm 1$ correspond to horizontally and vertically polarized photons propagating with well-defined momenta $\pm k$ along two distinct spatial directions ($\pm z$). We assume an initial vacuum state

$$|\psi\rangle_0 = |0\rangle_{+k,+1} |0\rangle_{-k,-1} \otimes |0\rangle_{+k,-1} |0\rangle_{-k,+1}, \quad (\text{S16})$$

with $|N_p\rangle_{\vec{k},m}$ being a Fock state in the corresponding pair modes. When quenching the couplings g_\pm for a time t , the Hamiltonian of Eq. (S15) generates a product state of two-mode squeezed vacuum states [17]

$$|\psi\rangle = |\psi_+\rangle \otimes |\psi_-\rangle, \quad (\text{S17})$$


with $|\psi\rangle_+ = \sum_{N_p=0}^{\infty} \sqrt{p_{\text{BE}}(N_p)} |N_p\rangle_{+k,+1} |N_p\rangle_{-k,-1}$, and $|\psi\rangle_-$ accordingly for the other channel χ_- . Using the mean pair number for each channel $\langle N_p^\pm \rangle = \sinh^2(g_\pm t)$ [18, 19], the coefficients of the different twin-Fock states contributing to $|\psi_\pm\rangle$ can be restated as $\sqrt{p_{\text{BE}}(N_p^\pm)} = \sqrt{1 - \tanh^2(g_\pm t)} \tanh^{N_p}(g_\pm t)$. Defining $\mu_\pm = \tanh(g_\pm t)$, we rewrite the two-mode squeezed vacuum states as

$$\begin{aligned} |\psi_+\rangle &= \sqrt{1 - \mu_+^2} \sum_{N_p^+=0}^{\infty} \mu_+^{N_p^+} |N_p^+\rangle_{+k,+1} |N_p^+\rangle_{-k,-1}, \\ |\psi_-\rangle &= \sqrt{1 - \mu_-^2} \sum_{N_p^-=0}^{\infty} \mu_-^{N_p^-} |N_p^-\rangle_{+k,-1} |N_p^-\rangle_{-k,+1}. \end{aligned} \quad (\text{S18})$$

For clarity, we consider first the case of small Zeeman splittings $\omega_z \rightarrow 0$, where both couplings $\mu_+ \approx \mu_- = \mu$ become equal. In this limit, we can explicitly write Eq. (S17) as

$$|\psi\rangle = (1 - \mu^2) \sum_{N_p^+, N_p^- = 0}^{\infty} \mu^{N_p^+ + N_p^-} |N_p^+, N_p^+; N_p^-, N_p^-\rangle, \quad (\text{S19})$$

where for conciseness we omit the labels for spin and momentum and identify the modes via their positions in



SI_histogram_v2.png

FIG. S2. Simulated pair statistics for vacuum and different classical seeds. (a) Pair histograms for short evolution times ($t = 30 \mu\text{s}$) and representative seeds of $N_p^s = 0$ (a1), 1 (a2) and 5 (a3). (b,c) Corresponding histograms for the experimentally relevant evolution time ($t = 60 \mu\text{s}$), directly obtained from the simulations (b) and after convolution with the technical detection noise (c). The mean and standard deviation for each distribution are marked by the purple bin and the black arrows, respectively. For the parameters of the truncated Wigner simulations, see Tab. S1 and Fig. 2(c) in the main text.

Eq. (S16). In the high gain-limit $\mu \rightarrow 1$, as considered in this work, the state of Eq. (S19) offers exciting possibilities for future experiments to study bipartite spin entanglement in spatially separated macroscopic atomic clouds along the drive $\pm z$ -direction, see also Ref. [20].

In the following, we focus on the low-gain limit $\mu \ll 1$, which opens up new avenues for prospective Bell tests with massive particles. Here, Eq. (S19) can be truncated to states corresponding to a single pair produced via ei-

ther channel:

$$|\psi\rangle \approx (1 - \mu^2) \left(|0, 0; 0, 0\rangle + \mu |1, 1; 0, 0\rangle + \mu |0, 0; 1, 1\rangle \right). \quad (\text{S20})$$

Since the vacuum state $|0, 0; 0, 0\rangle$ does not contribute to any of the measurements considered, we reduce the above state to

$$|\psi\rangle = \frac{1}{\sqrt{2}} \left(|1, 1; 0, 0\rangle + |0, 0; 1, 1\rangle \right), \quad (\text{S21})$$

The state of Eq. (S21) describes a pair of spin-entangled $m = \pm 1$ atoms propagating along $+z$ - and $-z$ -direction.

This state is analogous to a maximally polarization-entangled Bell state of two photons in two distinct spatial modes generated via SPDC [16]. Explicitly, we can identify the spin states $m = +1$ and $m = -1$ with the two polarization states horizontal (H) and vertical (V), respectively:

$$\begin{aligned} |1\rangle_{+1,+k} |0\rangle_{-1,+k} &\longrightarrow |H\rangle_z \\ |0\rangle_{+1,-k} |1\rangle_{-1,-k} &\longrightarrow |V\rangle_{-z} \\ |0\rangle_{+1,+k} |1\rangle_{-1,+k} &\longrightarrow |V\rangle_z \\ |1\rangle_{+1,-k} |0\rangle_{-1,-k} &\longrightarrow |H\rangle_{-z}. \end{aligned} \quad (\text{S22})$$

Therefore, Eq. (S21) can be rewritten as a Bell triplet state

$$|\psi\rangle_{\text{Bell}}^{\text{max}} = \frac{1}{\sqrt{2}} \left(|H\rangle_z |V\rangle_{-z} + |V\rangle_z |H\rangle_{-z} \right). \quad (\text{S23})$$

Finally, we consider the case of finite Zeeman splittings $\omega_z \neq 0$, where both couplings become unequal $\mu_+ \neq \mu_-$. The truncated state in the low-pair limit can then be written as

$$|\psi\rangle \sim \left(\mu_+ |1, 1; 0, 0\rangle + \mu_- |0, 0; 1, 1\rangle \right), \quad (\text{S24})$$

up to a normalization factor. The state of Eq. (S24) is analogous to a non-maximally entangled Bell state with tunable degree of entanglement via the couplings μ_{\pm} :

$$|\psi\rangle_{\text{Bell}}^{\text{non-max}} \sim \left(\mu_+ |H\rangle_z |V\rangle_{-z} + \mu_- |V\rangle_z |H\rangle_{-z} \right) \quad (\text{S25})$$

In SPDC, these states are generated through the rotation of the pump beam's polarization [21]. This rotation corresponds to manipulation of the magnetic field B in our system, which controls ω_z and thereby the coupling ratio μ_+/μ_- . Non-maximally entangled states play a crucial role in Bell tests, and they are especially important for addressing the detection loophole [22].

* These authors contributed equally to this work.

† donner@phys.ethz.ch

- [1] F. Schmidt, D. Mayer, M. Hohmann, T. Lausch, F. Kindermann, and A. Widera, Precision measurement of the Rb 87 tune-out wavelength in the hyperfine ground state $F = 1$ at 790 nm, *Physical Review A* **93**, 022507 (2016).
- [2] M. Landini, N. Dogra, K. Kroeger, L. Hruby, T. Donner, and T. Esslinger, Formation of a Spin Texture in a Quantum Gas Coupled to a Cavity, *Physical Review Letters* **120**, 223602 (2018).
- [3] B. Gadway, D. Pertot, R. Reimann, M. G. Cohen, and D. Schneble, Analysis of Kapitza-Dirac diffraction patterns beyond the Raman-Nath regime, *Opt. Express* **17**, 19173 (2009).
- [4] F. Ferri, R. Rosa-Medina, F. Finger, N. Dogra, M. Soriante, O. Zilberberg, T. Donner, and T. Esslinger, Emerging Dissipative Phases in a Superradiant Quantum Gas with Tunable Decay, *Physical Review X* **11**, 041046 (2021).
- [5] R. Rosa-Medina, F. Ferri, F. Finger, N. Dogra, K. Kroeger, R. Lin, R. Chitra, T. Donner, and T. Esslinger, Observing Dynamical Currents in a Non-Hermitian Momentum Lattice, *Physical Review Letters* **128**, 143602 (2022).
- [6] R. J. Fletcher, M. Robert-de Saint-Vincent, J. Man, N. Navon, R. P. Smith, K. G. H. Viebahn, and Z. Hadzibabic, Connecting Berezinskii-Kosterlitz-Thouless and BEC Phase Transitions by Tuning Interactions in a Trapped Gas, *Physical Review Lett.* **114**, 255302 (2015).
- [7] F. Brennecke, S. Ritter, T. Donner, and T. Esslinger, Cavity Optomechanics with a Bose-Einstein Condensate, *Science* **322**, 235 (2008).
- [8] C. Gross, H. Strobel, E. Nicklas, T. Zibold, N. Bargill, G. Kurizki, and M. K. Oberthaler, Atomic homodyne detection of continuous-variable entangled twin-atom states, *Nature* **480**, 219 (2011).
- [9] S. Hodgman, R. Khakimov, R. Lewis-Swan, A. Truscott, and K. Kheruntsyan, Solving the Quantum Many-Body Problem via Correlations Measured with a Momentum Microscope, *Physical Review Letters* **118**, 240402 (2017).
- [10] L. W. Clark, A. Gaj, L. Feng, and C. Chin, Collective emission of matter-wave jets from driven Bose-Einstein condensates, *Nature* **551**, 356 (2017).
- [11] F. Reiter and A. S. Sørensen, Effective operator formalism for open quantum systems, *Physical Review A* **85**, 032111 (2012).
- [12] P. Blakie, A. Bradley, M. Davis, R. Ballagh, and C. Gardiner, Dynamics and statistical mechanics of ultra-cold Bose gases using c-field techniques, *Advances in Physics* **57**, 363 (2008).
- [13] C. Mink, A. Pelster, J. Benary, H. Ott, and M. Fleischhauer, Variational truncated Wigner approximation for weakly interacting Bose fields: Dynamics of coupled condensates, *SciPost Physics* **12**, 051 (2022).
- [14] R. J. Lewis-Swan and K. V. Kheruntsyan, Proposal for a motional-state Bell inequality test with ultracold atoms, *Physical Review A* **91**, 052114 (2015).
- [15] K. F. Thomas, B. M. Henson, Y. Wang, R. J. Lewis-Swan, K. V. Kheruntsyan, S. S. Hodgman, and A. G. Truscott, A matter-wave Rarity-Tapster interferometer to demonstrate non-locality, *The European Physical Journal D* **76**, 244 (2022).
- [16] J.-W. Pan, Z.-B. Chen, C.-Y. Lu, H. Weinfurter, A. Zeilinger, and M. Żukowski, Multiphoton entanglement and interferometry, *Reviews of Modern Physics* **84**, 777 (2012).
- [17] S. L. Braunstein and P. van Loock, Quantum information with continuous variables, *Reviews of Modern Physics* **77**, 513 (2005).
- [18] D. Linnemann, H. Strobel, W. Muessel, J. Schulz, R. Lewis-Swan, K. Kheruntsyan, and M. Oberthaler, Quantum-Enhanced Sensing Based on Time Reversal of Nonlinear Dynamics, *Physical Review Letters* **117**, 013001 (2016).
- [19] A. Qu, B. Evrard, J. Dalibard, and F. Gerbier, Probing Spin Correlations in a Bose-Einstein Condensate Near the Single-Atom Level, *Physical Review Letters* **125**, 033401 (2020).
- [20] K. Lange, J. Peise, B. Lücke, I. Kruse, G. Vitagliano, I. Apellaniz, M. Kleinmann, G. Tóth, and C. Klempt,

Entanglement between two spatially separated atomic modes, [Science](#) **360**, 416 (2018).

- [21] A. G. White, D. F. V. James, P. H. Eberhard, and P. G. Kwiat, Nonmaximally Entangled States: Production, Characterization, and Utilization, [Physical Review Letters](#) **83**, 3103 (1999).
- [22] N. Brunner, D. Cavalcanti, S. Pironio, V. Scarani, and S. Wehner, Bell nonlocality, [Reviews of Modern Physics](#) **86**, 419 (2014).